Toxicology 504 (2024) 153783

Contents lists available at ScienceDirect

Toxicology

journal homepage: www.elsevier.com/locate/toxicol

Comparative toxicological analysis of two pristine carbon nanomaterials (graphene oxide and aminated graphene oxide) and their corresponding degraded forms using human *in vitro* models

Sandra de la Parra [a], Natalia Fernández-Pampín [a], Sebastiano Garroni [b], Matteo Poddighe [c], Dalia de la Fuente-Vivas [a], Rocío Barros [a], Sonia Martel-Martín [a], Santiago Aparicio [a,d], Carlos Rumbo [a,*], Juan Antonio Tamayo-Ramos [a,*,1]

[a] *International Research Center in Critical Raw Materials for Advanced Industrial Technologies-ICCRAM, Universidad de Burgos, Plaza Misael Bañuelos s/n, Burgos 09001, Spain*
[b] *Department of Chemical, Physics, Mathematics and Natural Science, University of Sassari, Via Vienna 2, Sassari 07100, Italy*
[c] *Laboratory of Materials Science and Nanotechnology (LMNT), Department of Chemical, Physics, Mathematics and Natural Science, CR-INSTM, University of Sassari, Via Vienna, 2, Sassari 07100, Italy*
[d] *Department of Chemistry, Universidad de Burgos, Burgos 09001, Spain*

ARTICLE INFO

Keywords:
A549 cells
HT29 cells
3D RhE model
Physical degradation

ABSTRACT

Despite the wide application of graphene-based materials, the information of the toxicity associated to some specific derivatives such as aminated graphene oxide is scarce. Likewise, most of these studies analyse the pristine materials, while the available data regarding the harmful effects of degraded forms is very limited. In this work, the toxicity of graphene oxide (GO), aminated graphene oxide (GO-NH_2), and their respective degraded forms (dGO and dGO-NH_2) obtained after being submitted to high-intensity sonication was evaluated applying *in vitro* assays in different models of human exposure. Viability and ROS assays were performed on A549 and HT29 cells, while their skin irritation potential was tested on a reconstructed human epidermis model. The obtained results showed that GO-NH_2 and dGO-NH_2 substantially decrease cell viability in the lung and gastrointestinal models, being this reduction slightly higher in the cells exposed to the degraded forms. In contrast, this parameter was not affected by GO and dGO which, conversely, showed the ability to induce higher levels of ROS than the pristine and degraded aminated forms. Furthermore, none of the materials is skin irritant. Altogether, these results provide new insights about the potential harmful effects of the selected graphene-based nanomaterials in comparison with their degraded counterparts.

1. Introduction

During the last years, carbon-based nanomaterials have been the object of intense research by the scientific and engineering communities. Due to their outstanding properties, these materials have emerged as excellent candidates for their application in a variety of areas, such as the electronic and automotive industries, or the biomedical and agricultural fields (Patel et al., 2019; Selvaraj et al., 2021; Sengupta, 2020; Zaytseva and Neumann, 2016). Graphene stands out among the different carbon-based nanomaterials, being extensively studied since its discovery in 2004 (Selvaraj et al., 2021) due to the unique properties conferred by its particular crystal structure, like excellent thermal and electrical conductivity, large specific surface area, high strength combined with high degrees of lightweight, and flexibility (Papageorgiou et al., 2017; Ren et al., 2018; Sattar, 2019). These characteristics have made graphene an exceptional material with great potential to be used in a broad range of fields and disciplines. In addition, graphene can be modified to obtain a wide portfolio of derivatives, including functionalized forms, which alter drastically its physicochemical properties, widening its potential applications. Graphene oxide (GO) is one of the most important graphene derivatives, as well as one of the most studied so far. This material can be obtained after the treatment of graphite with

* Corresponding authors.
E-mail addresses: crumbo@ubu.es (C. Rumbo), ja.tamayoramos@gmail.com (J.A. Tamayo-Ramos).
[1] Current affiliation: ITENE Research Center, Industrial Biotechnology Area, C/Albert Einstein 1, 46980, Paterna, Valencia, Spain.

https://doi.org/10.1016/j.tox.2024.153783
Received 22 December 2023; Received in revised form 18 March 2024; Accepted 19 March 2024
Available online 20 March 2024

strong oxidants, which finally leads to the formation of oxidized graphene layers presenting epoxy, hydroxyl, and carboxyl groups on their surface (Razaq et al., 2022). GO offers a series of advantages in comparison to graphene. First, its production is easier, and involves lower costs. In addition, its functional groups make GO highly hydrophilic allowing its good dispersibility in water and organic solvents (Ahmad et al., 2016; Paredes et al., 2008), and consequently facilitating its handling. Moreover, its oxygen-containing functional groups act as reactive sites, facilitating covalent bond functionalization on the nanomaterial's surface, and the further development of GO derivatives (Razaq et al., 2022; Yu et al., 2020). With regard to functionalized GO, many examples are found in the literature (Eivazzadeh-Keihan et al., 2022; He et al., 2010; Jing et al., 2015; Zhang et al., 2010). In particular, amine-functionalized GO is a promising nanomaterial with many potential applications in several fields. Hence, its improved electronic properties make this material a relevant candidate for photovoltaic or catalyst applications (Rabchinskii et al., 2020). Moreover, the increased reactivity and cytotoxicity against cancer cells described in the GO-NH_2 in comparison with non-functionalized GO has prompted the investigation of its potential use in anticancer therapies (Georgieva et al., 2020; Krasteva et al., 2019).

Since the introduction into the market of GO and some of its functionalized forms, their toxicological properties have been thoroughly investigated due to their potential hazard for humans and for the environment. Therefore, many research works have been carried out to study their safety applying different models (Amrollahi-Sharifabadi et al., 2018; Cebadero-Domínguez et al., 2022; Chang et al., 2011; Domi et al., 2020b; Shamsi et al., 2020; Zare-Zardini et al., 2018). Several studies have investigated the effects on different human cell lines after being exposed to pristine GO, showing that different parameters including their physicochemical characteristics or the cell type influence its toxicological properties. By the same token, *in vivo* experiments demonstrated that different aspects such as the surface coatings and size of the nanomaterials, as well as the administration route used in the experiments, determine the toxicity of GO, being the latter one of the most important factors (Yang et al., 2013). For instance, inhalation studies have shown that GO is able to cause minimal or inappreciable toxicity in the lungs and other organs (Han et al., 2015; Kim et al., 2018), while pulmonary exposure to this nanomaterial after intratracheal instillation induced inflammation, acute phase response and genotoxicity (Bengtson et al., 2017). However, the number of available studies addressing the safety of GO-NH_2 is low and, as mentioned above, given that the amination of GO seems to enhance its cytotoxicity in cancer cell lines, these works mainly analyse their potential role as anticancer compounds (Georgieva et al., 2020; Krasteva et al., 2019).

Another factor that should be considered when evaluating the harmful effects of graphene is its potential degradation during its lifespan. The intrinsic toxicity of nanoparticles depends on their physicochemical properties, such as size, shape, chemical composition, surface area and the chemical groups present on their surface (Sukhanova et al., 2018). These characteristics might be modified during their life cycle, and consequently their associated risks (Lowry et al., 2012). However, information about the safety of degraded nanomaterials, including graphene and its derivatives, is limited (Domi et al., 2020a; Fernández-Pampín et al., 2023), being most of the published studies focused on the risk assessment of pristine nanomaterials. In fact, only few research works have evaluated the potential hazard of GO degradation products after enzymatic or chemical treatments (Bortolozzo et al., 2021; Mukherjee et al., 2018), while in case of GO-NH_2, there is no available data about the potential pernicious effects of their degraded forms.

Considering the above explained, in the present study the toxicological impact of GO, GO-NH_2 and their respective degraded forms were evaluated and compared in representative models of human exposure through different routes (respiratory, gastrointestinal and dermal). The effect on the cell viability of different concentrations of both degraded and pristine nanomaterials, together with their ability to induce oxidative stress, were analysed in A549 (lung) and HT29 (intestine) cancer cell lines. In addition, the *In Vitro* EpiDerm Skin Irritation Test (EPI-200-SIT) was applied to study the effect of both degraded and pristine nanomaterials on the skin. Altogether, the obtained results provide new knowledge about the potential harmful effects of the degraded forms of different graphene derivatives in distinct human exposure scenarios.

2. Materials and Methods

2.1. Nanomaterials and sample preparation

GO and aminated GO (named as GO and GO-NH_2 respectively in this work) were provided by Graphenea (San Sebastián, Spain). To obtain the degraded forms of GO and aminated GO (named as dGO and dGO-NH_2 respectively in this work), the nanomaterials were previously suspended in ultrapure water up to a concentration of 4 mg/mL and subjected for 3 h of pulsed mode sonication (pulse duration: 5 s, rest: 2 s) using a Sonics tip sonicator, 20 kHz; 500 W, with a 30% of amplitude and a 13 mm diameter solid titanium tip. These parameters allow to keep the sonicated solution under moderate temperature, ensuring proper exfoliation of the nanomaterial while preventing thermal oxidation of the dispersed nanoparticles. Prior to toxicological analysis, the stocks (4 mg/mL) were further diluted in ultrapure water with 0.05% bovine serum albumin (BSA) to a concentration of 2.56 mg/mL, with the aim to facilitate their dispersion. They were then vortexed at maximum speed and sonicated using a Branson Sonifier Model SLPe cell disruptor continuously for 5 min, using 40% amplitude.

2.2. Physicochemical characterization of the pristine nanomaterials and their degraded counterparts

2.2.1. RAMAN analysis

Raman measurement was performed by a "Senterra" Raman microscope (Bruker) under a laser excitation of 532 nm (25.0 mW power). The spectra were collected with a resolution of $\approx$ 3–5 cm^{-1} and an integration time of 15 s. The sample (powder) was deposited on a silicon wafer and measurements were collected at room temperature.

2.2.2. TEM analysis

The morphological characteristics and size of the particles were analysed by Transmission Electron Microscopy (TEM) by the Microscopy Unit at the University of Valladolid. Before this analysis, the nanomaterials were dispersed in BSA (0.05%), sonicated in an ultrasonic bath for 5 minutes, and deposited in a Lacey Carbon Type-A, 300 mesh, copper grid. Samples were visualized and photographed using a JEOL JEM-1011 HR TEM coupled with a Gatan Erlangshen ES1000W camera.

2.2.3. ICP-MS

In order to analyse the ion releasement, aqueous suspensions were obtained by subjecting the initial stocks (4 mg/mL) to a centrifugation and filtration process, using filters with a pore size of 0.2 μm. The centrifugation conditions applied were different (4500 rpm 20 min for GO and dGO and 13000 rpm 30 min for GO-NH_2 and dGO-NH_2), due to the difficulty in sedimentation shown by the samples functionalized with amino groups. Then, these filtered supernatants were analyzed by inductively coupled plasma mass spectrometry (ICP-MS) using an Agilent 8900 ICP-QQQ at the University of Burgos. Five replicates were used for data acquisition.

2.3. Cell lines and culture conditions

The human alveolar carcinoma epithelial cell line (A549) was cultured in commercial Dulbecco's Modified Eagle's Medium (DMEM) supplemented with 10% fetal bovine serum (FBS) and 1% penicillin/streptomycin. The human colon cancer cell line (HT29) was grown in

commercial McCoy's medium supplemented with 10% FBS, 1% L-glutamine and 1% penicillin/streptomycin. Both cell cultures were kept in a thermostatic incubator under optimal growth conditions (humidified atmosphere containing 5% CO_2 and 37 °C).

2.4. Toxicology assays

2.4.1. Experiments using A549 and HT29 cell lines

The ability of GO, dGO, GO-NH_2, and dGO-NH_2 to affect the cell viability and induce reactive oxygen species (ROS) formation in A549 and HT29 cells was determined exposing both cell lines to 10 and 20 mg/L of the materials. These concentrations are closer to realistic doses of human exposure, and within the recommended concentrations range to be used in the submerged settings to avoid nanomaterials agglomeration and sedimentation (Drasler et al., 2017).

2.4.1.1. MTT Assay. A549 and HT29 cells were seeded in 96-well plates at 5×10^3 and 10×10^3 cells per well, respectively. Both were treated with 10 and 20 mg/L of the materials diluted in their appropriate culture medium supplemented with 1% FBS. As controls, cells incubated with culture medium alone (live cells control) and cells treated with water (dead cells control) were used. 24 h after exposure, the culture medium with the materials was withdrawn, and cells were washed with Dulbecco's Phosphate-Buffered Saline (DPBS) and 100 μL of a solution of MTT (3-(4,5-dimethylthiazol-2-yl)-(2,5-diphenyltetrazolium bromide) at 500 mg/L were added to each well, and incubated for 3 h. After this time, the solution medium was discarded, and 100 μL of dimethyl sulfoxide (DMSO) was added to solubilize the formazan crystals by gentle shaking for 15 min. Finally, the absorbance was measured with a microplate reader (BioTek Synergy HT, OD 590 nm). Data represent the mean of two independent experiments with at least three biological replicates. The absence of interference between the nanomaterials and the MTT to produce formazan was confirmed under cell-free conditions (Supplementary Material, S1; Figure S1).

2.4.1.2. Oxidative stress assay. The quantitative assessment of intracellular ROS was studied using the 2,7-dichlorofluorescein diacetate (DCFH-DA). A549 and HT29 cells were seeded in 96-well plates at 3×10^4 cells per well and incubated in optimal growth conditions for 24 h. After this time, cells were washed with Hanks Balanced Salt solution (HBSS) and incubated with 50 μM DCFH-DA in HBSS for 30 min at 37 °C in darkness. Then, cells were washed once with HBSS and exposed to 10 and 20 mg/L of the materials diluted in HBSS. Cells incubated with HBSS alone were used as negative control, and cells treated with H_2O_2 were used as a positive control. Fluorescence was measured using a microplate reader (BioTek Synergy HT, excitation wavelength, 485/20; emission wavelength 528/20) after incubating 60 min. Data represent the mean of two independent experiments with at least three biological replicates each. Prior to this test, the interference of the nanomaterials with DCF was evaluated (Supplementary Material, S2; Figure S2, Table S1).

2.4.2. In Vitro EpiDerm Skin Irritation Test

To study the irritant potential of the materials over the skin, the *In Vitro* EpiDerm Skin Irritation Test, EPI-200-SI (MatTek) was applied following the manufacturer's recommendations. Briefly, after the preparation and stabilization steps, the tissues were topically exposed to the nanomaterial suspensions at 1 mg/mL for 60 min. Three tissues were used per test material and controls (negative control: tissues exposed to DPBS; positive control: tissues exposed to a 5% solution of SDS in water). The percentage of viable cells after material exposure was determined using the MTT viability assay. Before performing this test, the non-interaction of the nanomaterials with the MTT was confirmed following the guideline suggestions. This test fulfils criteria of OECD TG 439.

2.5. Statistical analysis

Statistical analysis data are presented as means ± standard deviation (SD). The Kolmogorov-Smirnov test was applied to analyse the normality of the data. The one-way analysis of variance (ANOVA) was used for multiple comparison test, followed by Tukey *post hoc* test to compare every mean with the control and with the other samples. Statistical tests were carried out using Prism 8.0 (GraphPad Prism, GraphPad Software, Inc.). Differences were considered significant at $P \leq 0.05$.

3. Results

3.1. Characterization of the materials

In the present study, two graphene-derived nanomaterials (GO and GO-NH_2) and their respective degraded forms were analyzed from a safety perspective. Prior to their toxicological evaluation, the nanomaterials were physicochemically characterized through several techniques. First, the morphology and size of the particles were analyzed by TEM, as both are physical attributes that can influence the toxicity degree of the different types of graphene. TEM analysis showed that GO and GO-NH_2 present a sheet-like morphology, being GO nanoparticles larger than those from GO-NH_2 (Fig. 1). Areas that show high electron density are observed mainly in the center of the particles, suggesting the presence of several layers with functional groups. In the periphery of the sheets, higher transparent areas are distinguished, which might be indicative of the existence of few or thinner layers. Regarding the degraded materials, they present substantial morphological differences in comparison to their pristine counterparts. In the case of dGO, a reduction in the size of the particles is observed, being those more transparent and, therefore, indicating the presence of a fewer number of layers. Moreover, a dark coating can be noticed throughout the sample, which is probably related to the finest remnants produced during the degradation process. Regarding dGO-NH_2, these particles show a complete loss of morphology, as well as a significant reduction in their size. In addition, they have a crumbled-like appearance and, as in the GO degraded sample, the sheets are less electron-dense than their corresponding non-degraded forms.

The structure and stoichiometry of the pristine and ultrasound-treated (degraded) nanomaterials were also analyzed by Raman. Fig. 2 shows the Raman spectra collected on the GO and GO-NH_2 samples, obtained under a laser excitation of 532 nm and a power of 25.0 mW. As it can be observed in Fig. 2(a), a non-significant difference is observed between the untreated (black line) and the ultrasound-treated (red line) GO-NH_2 samples. Monitoring the spectra, the presence of a shoulder (D′-Peak) on the G-Peak, typically associated with anomalies on the sample surface, could not be observed (DiLeo et al., 2007; Jorio et al., 2003). Also, the 2D band at 2680 cm^{-1} does not show any significant change upon ultrasonic treatment, indicating poor exfoliation of the sample (Ferrari et al., 2006). In contrast, Fig. 2(b) shows more intense and narrow peaks for dGO due to the effect of sonication. The peak at 1570 cm^{-1} (G-Peak) may contribute to reveal the crystallinity of the sample. Besides, the peaks at 1338 and 1608 cm^{-1} (D-Peak and D'-Peak, respectively) indicate the presence of irregularities on the sample surface. These may be caused by the presence of crystallite boundaries, impurities, or sp^3 hybridized carbons formed during particle fracture as result of sonication. In addition, the 2D band at about 2675 cm^{-1} is slightly more intense and narrow after ultrasound treatment, indicating higher exfoliation of the sample. The background of the Raman data was processed for the purpose of fitting the spectral intensity basing on Lorentzian functions. The intensity of the D and G peaks, in sample GO-NH_2, were calculated, resulting in an I_D/I_G ratio of ~1.19. According to Wróblewska *et al.*, this ratio is close to the one of GO (1.21) (Wróblewska et al., 2017), while after ultrasound treatment it is obtained a ratio I_D/I_G to the ~0.73, suggesting the GO state is an

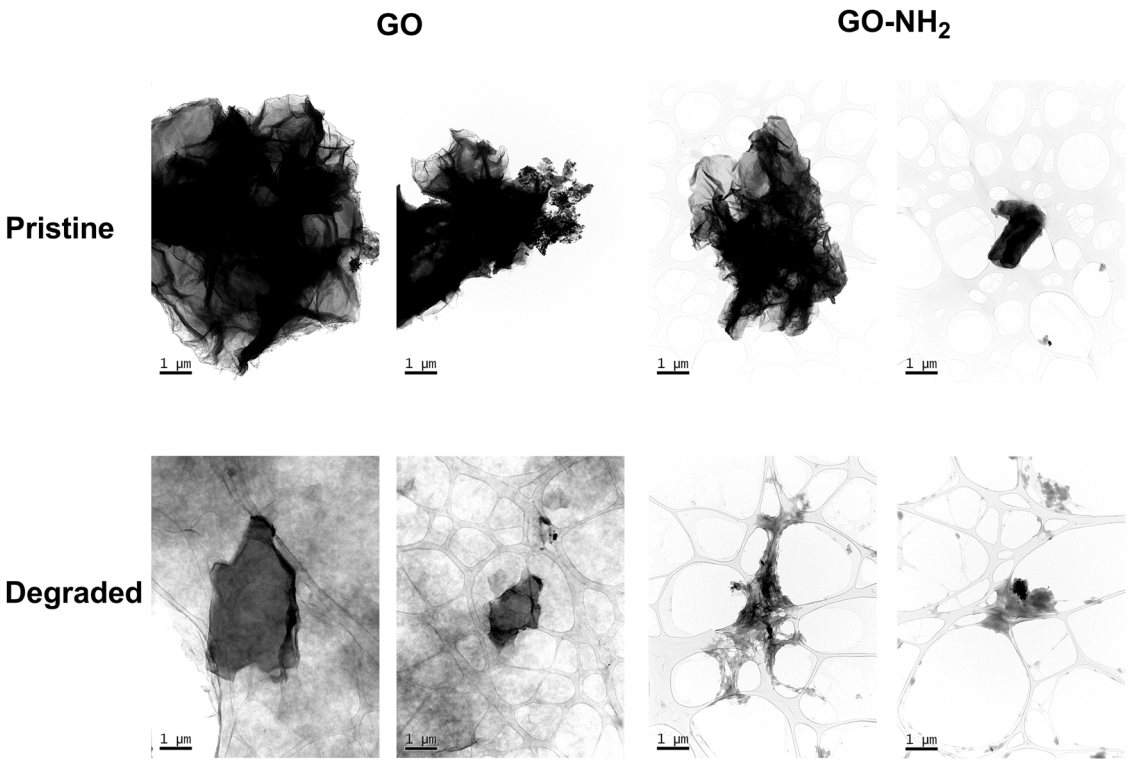

Fig. 1. : TEM analysis of GO, GO-NH_2, dGO and dGO-NH_2: Original magnification × 20000 (scale bar = 1 µm). Graphene suspensions with a final concentration of 4 mg/mL were deposited on a Lacey Carbon copper grid.

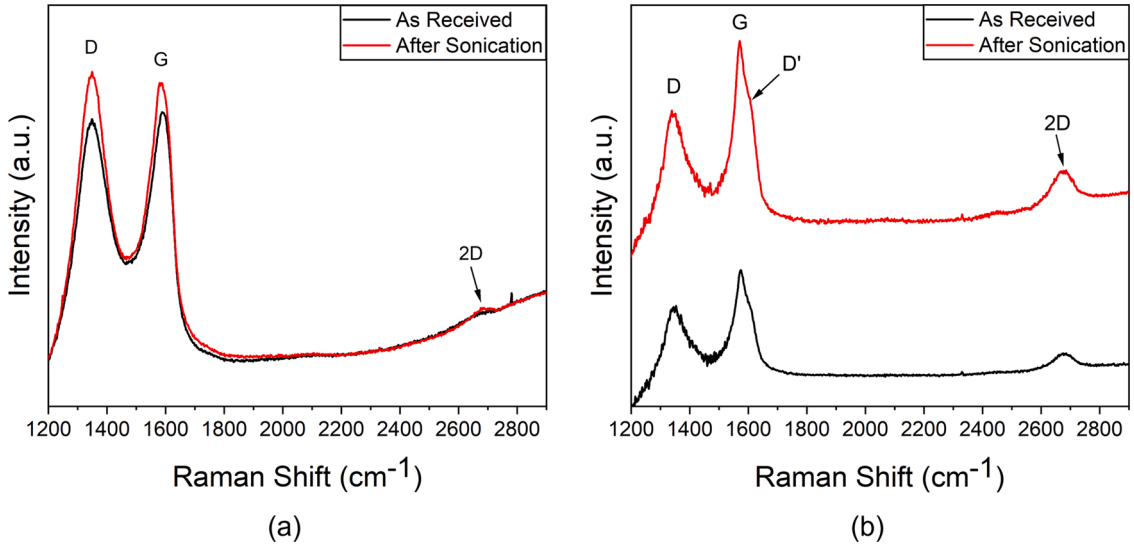

Fig. 2. : Raman spectra in the range 1200–2900 cm^{-1} of (a): GO-NH_2 and (b): GO samples. Characteristic peak of the crystalline structure of the samples can be observed at 1586 and 1570 cm^{-1} (G-Peak) of GO-NH_2 and GO, respectively; the peak at 1349 cm^{-1} (D-Peak of GO-NH_2) and the peaks at 1338 cm^{-1} and ~1608 cm^{-1} (D-Peak and D′-Peak respectively of GO) indicate the presence of defects on the surface of the sample. The 2D band (at about 2680 cm^{-1} in both GO samples) determines the graphene layer thickness.

intermediate between unexfoliated graphene (0.02) and the GO (Saiful Badri et al., 2017).

In order to detect the possible presence of trace metals in the filtered supernatants of the pristine and degraded materials suspensions, trace element analysis was performed by ICP-MS. As shown in Table 1, several metallic elements were detected in GO and GO-NH_2 samples, most of them present in low concentrations. GO and dGO supernatants showed higher metal concentrations than those of GO-NH_2 and dGO-NH_2 and, in general terms, their degradation did not induce the release of metal ions. Mn and S concentrations are particularly higher in the case of GO and its degraded counterpart in comparison with the aminated forms, suggesting that the Hummer method was used for the chemical oxidation to produce this material. Through this method, graphite flakes react with a mixture of sulphuric acid (H_2SO_4), sodium nitrate ($NaNO_3$) and potassium permanganate ($KMnO_4$), which can lead to residual accumulation of Mn and S, thus explaining their relevant presence in the studied GO nanomaterials (Liao et al., 2018). In the case of the GO-NH_2 and dGO-NH_2 supernatants, the presence of low concentrations of both

Table 1
Trace metals detected by inductively coupled plasma mass spectrometry (ICP-MS) analysis of GO, dGO, GO-NH_2 and dGO-NH_2 supernatants. Values below the detection limit of the ICP-MS procedure are also shown. "ND" stands for "under detection limit".

Elements (ppm)	GO	dGO	GO-NH ₂	dGO-NH ₂
Al	0.004	0.121	<0.003	0.008
Cr	ND	0.001	ND	ND
Cu	0.001	0.001	0.001	0.001
Fe	0.007	0.010	0.004	0.004
K	0.692	0.711	0.084	0.098
Mg	0.009	0.012	0.015	0.026
Mn	10.299	12.774	0.092	0.997
Mo	ND	ND	ND	0.001
Ni	0.004	0.005	0.004	0.004
Rb	0.001	0.001	ND	ND
S	24.297	25.128	1.831	1.854
Ti	ND	0.011	ND	0.011
V	ND	0.039	ND	0.003
Zn	0.039	0.024	0.004	0.011

elements in comparison with those present in GO and its degraded counterpart supernatants, could be attributed to the synthesis process applied, in which the GO is conjugated with NH_2 groups and subsequently purified, leading to a loss of metals.

3.2. Determination of A549 and HT29 cells response to GO, dGO, GO-NH_2 and dGO-NH_2

The viability of A549 and HT29 human cancer cell lines after 24 h of exposure to 10 and 20 mg/L of GO, dGO, GO-NH_2, and dGO-NH_2 was determined by the MTT assay. This assay is a colorimetric test used to evaluate the cell metabolic activity, and it is based on the ability of the active viable cells to transform MTT into a purple formazan product that can be measured at OD 590 nm. As can be seen in Fig. 3, no effect was observed on the viability of the A549 cells when exposed to any of the concentrations of GO and dGO, showing in all cases similar percentages of viable cells to those of the control. Nevertheless, cells exposed to a GO-NH_2 and dGO-NH_2 showed a statistically significant viability decrease in comparison to the non-treated cells. In the case of GO-NH_2, this parameter was reduced ≈ 24% and ≈ 30% when exposed to 10 and 20 mg/L of the nanomaterial, respectively. In the same way, exposure to dGO-NH_2 resulted in a loss of viability of approximately ≈ 40% at both concentrations.

The ability of these nanomaterials to induce ROS formation was also assessed after 1 h of exposure to 10 and 20 mg/L, using the DFCH-DA fluorophore test. The interference assay of the nanomaterials with DCF showed a slight statistically significant decrease in the fluorescence in the case of GO and dGO at 20 mg/L. Thus, a correction factor was calculated and applied (relative fluorescence value experimentally obtained × 1.25) (Supplementary Material, S2; Figure S2; Table S1). Fig. 4 shows that A549 cells present a statistically significant increase in ROS levels when exposed to GO, dGO, and GO-NH_2, being this induction much higher in the first two cases. Furthermore, it was observed that cells exposed to the higher concentrations of the nanomaterials induce higher levels of ROS in a clear dose-response relationship. However, the exposure to dGO-NH_2 did not result in a statistically significant increase in the ROS production when compared to the control.

Both viability and oxidative stress assays were also performed in the HT29 cell line after being exposed to the same nanomaterials concentrations. Regarding the MTT assay, the results reveal that, after 24 h of exposure to GO and dGO, there were non-negative effects on cell viability at any of the concentrations tested, showing all the studied conditions similar percentages of viable cells (Fig. 5). On the contrary, a statistically significant reduction in this parameter was observed in cells exposed to GO-NH_2 and dGO-NH_2. In the case of GO-NH_2, a viability decrease of ≈ 22% was observed at 10 mg/L and ≈ 26% at 20 mg/L of the nanomaterial concentration. In the same way, exposure to 10 and 20 mg/L of dGO-NH_2 produced a viability loss of ≈ 39% and ≈ 44%, respectively.

Concerning the ability of these nanomaterials and their respective degraded counterparts to induce ROS in the HT29 cell line, Fig. 6 shows the results obtained after 1 h of exposure (relative fluorescence values obtained in cells exposed to both GO and dGO at 20 mg/L were also corrected as explained above). In this case, the oxidative stress induction was notably increased during the exposure to all the tested concentrations of GO, dGO and GO-NH_2 in a dose-response relationship, being ROS levels statistically significant in all cases, and remarkably higher in cells exposed to GO and dGO. In contrast, in cells exposed to dGO-NH_2 only a statistically significant increase in the ROS production was observed at 20 mg/L when compared to control.

3.3. Determination of skin irritant response to GO, dGO, GO-NH_2 and dGO-NH_2

The irritation potential of GO, GO-NH_2, and their respective

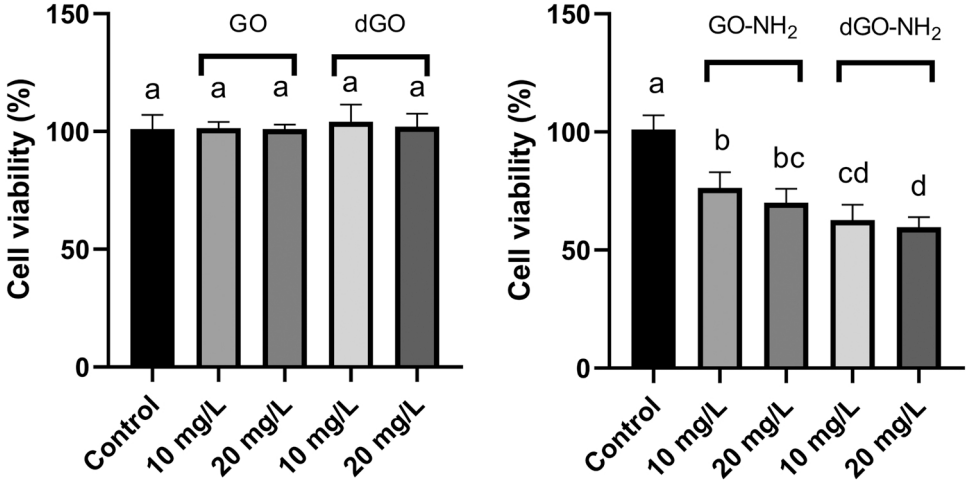

Fig. 3. : Viability of A549 cells treated with different concentrations of GO and dGO (left) and GO-NH_2 and dGO-NH_2 (right). Results are expressed as a percentage of control (untreated cells). Data represent the mean (± standard deviation, SD) of at least 6 biological replicates obtained in two independent assays. Differences are established using a one-way ANOVA followed by a multicomparison test (Tukey test), and considered significant when $P \leq 0.05$. Different letters indicate significant differences between treatments.

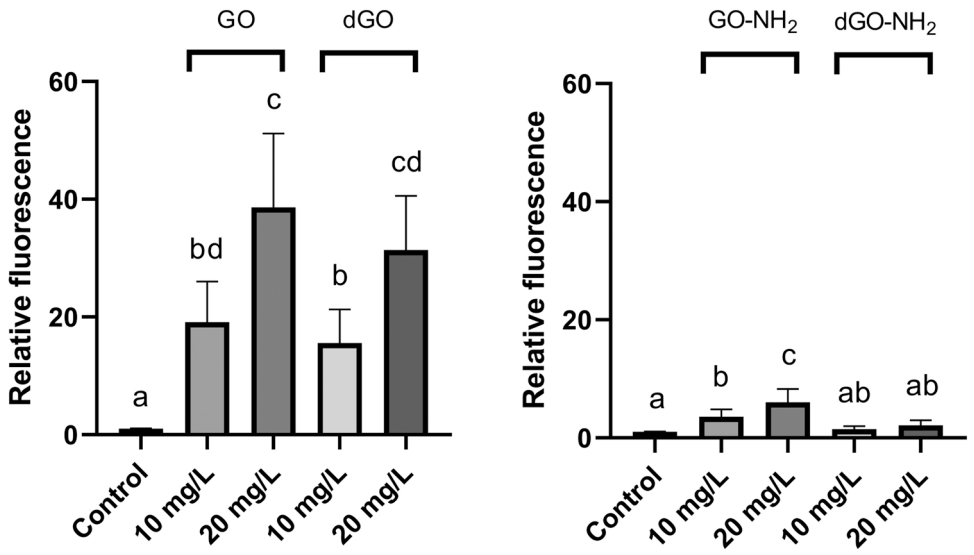

Fig. 4. : Reactive oxygen species (ROS) production of A549 cells treated with different concentrations of GO and dGO (left) and GO-NH_2 and dGO-NH_2 (right). Results are expressed as the relative fluorescence value to the control (untreated cells), which was assigned a value of 1. Data represent the mean (± standard deviation, SD) of at least 6 biological replicates obtained in two independent assays. Differences were established using a one-way ANOVA followed by a multi-comparison test (Tukey test), and considered significant when $P \leq 0.05$. Different letters indicate significant differences between treatments.

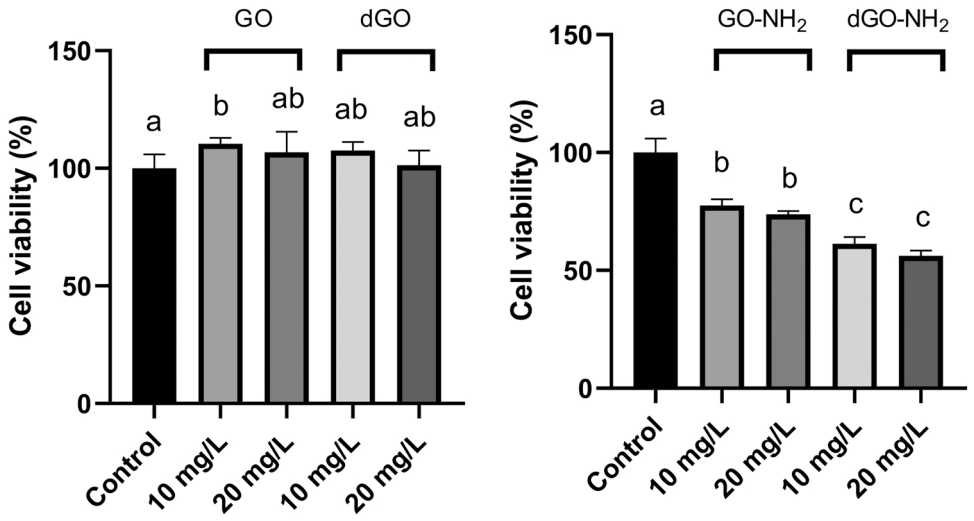

Fig. 5. : Viability of HT29 cells (MTT assay) treated with different concentrations of GO and dGO (left) and GO-NH_2 and dGO-NH_2 (right). Results are expressed as percentage of control (untreated cells). Data represent the mean (± standard deviation, SD) of at least 6 biological replicates obtained in two independent assays. Differences were established using a one-way ANOVA followed by a multicomparison test (Tukey test), and considered significant when $P \leq 0.05$. Different letters indicate significant differences between treatments.

degraded forms was evaluated under OECD guidelines (Test No. 439) using the *In Vitro* EpiDerm Skin Irritation Test (EPI-200-SIT). As described in the corresponding Materials and Methods section, the test is based on a topical exposure of the nanomaterials to a reconstructed human epidermis (RhE) model, which consists of a 3D cell culture closely mimicking the biochemical and physiological properties of the upper parts of the human skin, followed by the determination of cell viability by MTT assay.

The tissues were exposed to 1 mg/mL of the nanomaterials. Fig. 7 shows that only the degraded forms reduce approximately 20% the viability of RhE with respect to the control (tissues exposed to PBS), but these differences are not statistically significant. In contrast, the pristine nanomaterials do not affect the RhE viability. Thus, none of the nanomaterials studied showed to have irritation potential, neither their pristine forms nor their degraded counterparts. By the same token, tissues directly exposed to pristine nanomaterials powders did not result in a negative effect (supplementary material, Figure S3).

4. Discussion

The increased use of nanoparticles in several fields has raised concerns about the potential hazard effects that these nanomaterials can represent for human health and for the environment once they are released. In particular, graphene-based nanomaterials stand out due to their exceptional physicochemical properties, being applied in a variety of areas, and thus many research works focused on the evaluation of their toxicity are available in the current literature (Achawi et al., 2021; Rhazouani et al., 2021). As explained above, the toxicity of nanoparticles is determined by different physicochemical characteristics including chemical composition, geometry or shape (Sukhanova et al., 2018). Inevitably, these properties can be drastically altered once they are released into the environment, where they are subjected to different

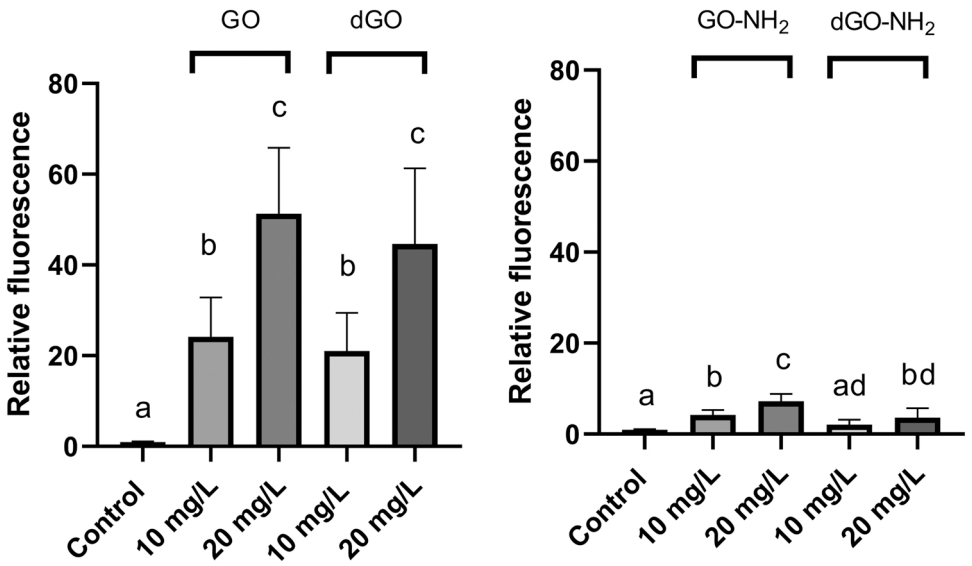

Fig. 6. : Reactive oxygen species (ROS) production of HT29 cells treated with different concentrations of GO and dGO (left) and GO-NH_2 and dGO-NH_2 (right). Results are expressed as the relative fluorescence value to the control (untreated cells), which was assigned a value of 1. Data represent the mean (± standard deviation, SD) of at least 6 biological replicates obtained in two independent assays. Differences were established using a one-way ANOVA followed by multi-comparison test (Tukey test), and considered significant when $P \leq 0.05$. Different letters indicate significant differences between treatments.

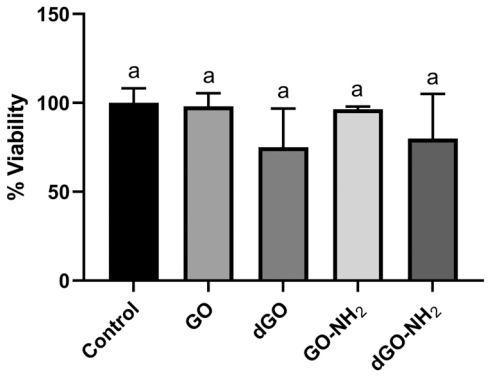

Fig. 7. : EpiDerm tissues were exposed to 1 mg/mL of GO, dGO, GO-NH_2 and dGO-NH_2. The viability was analysed by MTT assay, and it is expressed as a percent of negative control (tissues exposed to PBS). Data represent the mean ± standard deviation (SD). Differences were established using a one-way ANOVA followed by a multiple comparisons test (Tukey test), and considered significant when $P \leq 0.05$. Different letters indicate significant differences between treatments.

factors such as those associated to climatic events (sunlight, heat, humidity, or general wear and tear) and, consequently, their hazard potential could be modified (Domi et al., 2020a). In spite of the relevance of this issue, the number of works addressing the implications of the degradation in the inherent toxicological properties of the nanomaterials is scarce. Thus, providing information about how the structural and composition changes caused by the degradation of these materials influence their potential toxicity is a matter of concern that should be addressed, which allow to better understand the hazards associated to a particular nanomaterial. In the present work, two graphene-derived nanomaterials (GO and GO-NH_2) and their respective degraded forms obtained after severe physical degradation were evaluated.

Inhalation, dermal contact and ingestion are the most common routes of exposure to nanoparticles. In the specific case of graphene-based materials, their associated risk is especially relevant in the occupational exposure context, which involves the whole life cycle of the product, from production to waste disposal stages (Park et al., 2017). Different reviews have analysed in depth the most common pathways of graphene-based materials entry to the human body (Fadeel et al., 2018; Pelin et al., 2018; Rhazouani et al., 2021). Briefly, inhalation is considered as the highest concern-route, since the volatility of these materials when being in powder form make them potentially dangerous for lungs. The skin also constitutes one of the most relevant exposure routes, having a key role as barrier between the human body and the environment, and being one of the most susceptible organs to accidental exposure too. Finally, oral exposure is also significant, since graphene-based materials can reach the gastro-intestinal tract by direct ingestion or due to transportation of inhaled materials to oral cavities, where they can be swallowed. Based on the above, different representative human models for lung (A549 cells), intestine (HT29 cells) and skin (RhE) exposure were selected to perform the toxicological evaluation of the selected compounds. The A549 cell line is considered a steady model for human alveolar type II pulmonary epithelium and it is commonly used for the evaluation of pulmonary toxicity of nanoparticles (Bacova et al., 2022), including graphene-based nanomaterials (Chang et al., 2011; Domi et al., 2020b). In the case of the HT29 cell line, it is widely applied as model for evaluating the effects of food contaminants after oral uptake (del Rio et al., 2017; Linares et al., 2016), as well as those caused by nanoparticles (Schneider et al., 2017; Sergent et al., 2012). Finally, reconstructed human epidermis models are advanced systems that consist of a fully differentiated epidermis resembling the human skin. Regarding the parameters under study, ROS production was chosen together with viability determination to evaluate the toxicological potential of the nanomaterials in both A549 and HT29 cell lines. ROS increment is a common feature of GO toxicity, involved in several cellular damage processes such as lipids degradation, DNA fragmentation, or protein denaturation (Rhazouani et al., 2021). Regarding the experiments carried out with the RhE model, irritation could be considered as the most feasible effect on this organ due to the chemical nature of graphene-based materials (Fadeel et al., 2018), so this parameter was evaluated in this study.

4.1. Physicochemical properties of pristine and degraded nanomaterials

Firstly, both pristine and degraded nanomaterials were physicochemically characterized using different techniques. Raman analysis showed non-significant differences between the spectra of pristine and

degraded GO-NH_2, while in the case of GO, its ultrasonicated counterpart displayed more intense and narrow peaks. The modifications caused by the sonication in both nanomaterials were more evident by TEM analysis. In general terms, the degraded nanoparticles showed a reduced size and less electron-dense areas, indicative of fewer number of layers. In addition, in the case of the dGO-NH_2, the loss of morphology was more marked than in the dGO, while the latter samples showed a dark coating that could be associated to finest remnants produced during the sonication. Regarding the metal ions release, no significant alterations in their levels were observed in the suspensions after the degradation process. Only an increase in the levels of Al and Mn were detected in dGO and dGO-NH_2 supernatants respectively, being very low concentrations in any case. The presence of Mn impurities on GO samples is considered a relevant factor due to the ability of this element to induce significant biological effects (Seabra et al., 2014). In our work, it is important to remark that the levels of Mn present in the highest concentration used in the toxicological assays are 200 times lower than those reported in Table 1 ($\approx$ 0.05 ppm in the case of cells exposed to 20 mg/L of GO and dGO). Some authors have observed certain toxic effects of low concentrations of Mn (0.1 mg/L) in different cell lines such as CHO-XRS5 cells or peripheral blood mononuclear cells (Francisco et al., 2023, 2021). On the other hand, in a previous work performed in our lab, the viability of HepG2 cells was not negatively affected when exposed to soil soluble extracts containing mixtures of metals at concentrations higher than those reported here (specifically, Mn was detected at $\approx$ 0.1 and $\approx$ 0.9 mg/L in two soil extracts respectively) (de la Parra et al., 2022). To our knowledge, no previous works evaluated the safety of concentrations as low as those detected in our samples so, although it can not be totally dismissed, its effect on the toxicity is probably insignificant in comparison to that caused by the particles *per se*.

4.2. Effect of pristine GO and GO-NH_2 on A549 and HT29 cell lines

The toxicological potential of pristine GO in different human cell lines has been evaluated in several studies but, as described by different reviews, the results reported in the literature on biocompatibility and toxicity are sometimes conflicting (Chiticaru and Ionita, 2022; Liao et al., 2018; Rhazouani et al., 2021). These discrepancies could be attributed to the influence of parameters such as size, surface chemistry, presence of impurities, etc. Moreover, as observed with other nanoparticles such as SiO_2 or TiO_2 (Sohaebuddin et al., 2010), the toxicological response after GO exposure is variable between cell types (Dąbrowski et al., 2023; Liao et al., 2018). In the present work, the results obtained in A549 cells are in agreement with those reported by other authors, where GO exposure showed to generate only a minimal loss of viability at high concentrations, while this nanomaterial is able to induce oxidative stress even at low concentrations (Chang et al., 2011; Domi et al., 2020b). By contrast, other authors observed a size and dose dependent effect on A549 cells, being GO able to highly decrease the percentage of viable cells at high concentrations after 24 hours of exposure (Gies and Zou, 2018). Nevertheless, this study agrees with the results reported here in establishing that low concentrations of GO do not negatively affect the viability of this cell line. Regarding studies reporting the effect of GO in gastro-intestinal cells, a number of works have been published (Feng et al., 2022; Krasteva et al., 2019; Kucki et al., 2016). In the specific case of HT29 cells, recently, Vimalanathan *et al.* showed that GO displays significant dose-dependent cytotoxicity on these cells even at low concentrations similar to those used in the present study (Vimalanathan et al., 2022). However, other authors observed that when this cell line is present in a co-culture with Caco-2 cells, no cytotoxic effects in terms of viability or oxidative damage were detected, while moderate genotoxic effects were observed after 24 h of exposure at different concentrations of GO (Domenech et al., 2020). Furthermore, it has been reported that GO can constitute a great support for HT29 cell attachment, growth, and proliferation (Ruiz et al., 2011). The results being reported in the present study indicate that, in spite of the fact that the viability of HT29 cells is not affected, GO is able to cause some cytotoxic features (ROS production). Altogether, the obtained data reveal the need of performing further research in order to generate additional knowledge on the effect of GO in gastrointestinal cells. While an extensive work has been done in unveiling the potential toxicity of GO for different cellular models, the number of research works investigating the toxicological effects produced by aminated GO is much lower. In the current work, tests performed with GO-NH_2 in both cell lines show a statistically significant decrease in cell viability, as well as statistically significant levels of ROS, with the concentrations tested. These results are in concordance with those previously reported, where the functionalization of GO with amino groups was associated to cytotoxicity and genotoxicity induction upon nanoparticle exposure in both lung and gastro-intestinal cell lines (Keremidarska-Markova et al., 2018; Krasteva et al., 2019). The fact of observing an increase in the ROS levels of cells exposed to GO, without affecting their viability after 24 hours of exposure is intriguing. However, this phenomenon was also described in the above-mentioned research studies where the toxicity of GO was evaluated (Chang et al., 2011; Domi et al., 2020b). This could be indicative of the activation of cell mechanisms that help to overcome oxidative stress, such as the action of antioxidant enzymes able to mitigate ROS effects (Jena et al., 2023) or the induction of autophagy, which can be considered as an antioxidant repairing system since it can contribute eliminating the damaged oxidized biomolecules (Filomeni et al., 2015). In the case of cells exposed to GO-NH_2, our observations suggest that ROS could play a relevant role in the decrease of viability. These results are in line with those described by Krasteva *et al.*, who reported an increment in ROS production, together with other cytotoxic effects, after exposing Colon-26 cell line to GO-NH_2 (Krasteva et al., 2019). To our knowledge, no previous work evaluated the effect of aminated GO in the HT29 cell line.

4.3. Effect of dGO and dGO-NH_2 on A549 and HT29 cell lines

As previously mentioned, the number of studies evaluating the toxicological effect of degraded nanoparticles is scarce. In particular, there is very limited information about the influence of physical degradation in graphene-based materials toxicity, being a previous work performed in our laboratory one of the first studies where the degradation of graphene derivatives (i.e. graphene functionalized with MnOx nanoparticles) has been simulated, followed by their toxicological properties determination (Fernández-Pampín et al., 2023). During the physical degradation process, modifications can occur in the structure and composition of the nanomaterials (decrease in the thickness of the layers, morphology changes, etc.), thus generating a possible alteration of their toxicological potential. Therefore, to increase knowledge about the influence of physical degradation on the properties of the nanomaterials under study, GO and GO-NH_2 were subjected to the same prolonged sonication process described in our previous work (Fernández-Pampín et al., 2023), and their toxicological potential was assessed in the same conditions as for the pristine materials. The obtained results showed that the degradation of GO did not alter their toxicological properties, presenting similar effects than the pristine nanomaterial. In the case of dGO-NH_2, the effects were also similar to those observed with their pristine counterpart, showing to cause a slightly higher decrease in the viability, but lower levels of ROS. This fact could indicate a greater involvement of a ROS independent pathway in the toxicity induced by dGO-NH_2, as for example, the physical interaction with the nanostructures of the cells such as the actin cytoskeleton, or through cell cycle arrest. Both mechanisms were previously described as ROS independent pathways induced by nanoparticles (Shvedova et al., 2012). The morphology of the sheets is among the parameters that can greatly affect the toxicity and biocompatibility of graphene-based materials (Gurunathan et al., 2019; Ou et al., 2016). In fact, some studies have associated the presence of extremely sharp edges with cytotoxicity

through the destabilization of the membrane and subsequent cell integrity loss (Lalwani et al., 2016). Moreover, Chang *et al.* observed GO size-dependent toxicity in A549 cells when the materials are in the nanometric scale (Chang et al., 2011). In the present work, in terms of cell viability and ROS production, the significant differences observed in the shape and size of the nanomaterials after the application of the degradation protocol did not show to substantially influence their toxicological potential. In the case of the GO-NH_2, the slightly higher viability reduction observed in the cells exposed to the degraded forms in comparison with that caused by the pristine counterpart could be, in some degree, related with the sharped edges observed in dGO-NH_2 but, in any case, these modifications seem not to be critical.

4.4. Effect of GO, GO-NH_2 and their degraded counterparts on skin tissues

The skin is one of the main routes of exposure to nanoparticles, so the effect of graphene-derived nanomaterials suspensions and powders on this organ was evaluated using the 3D RhE model, an advanced system that consists of a fully differentiated epidermis resembling the human skin tissue. The obtained results showed that GO, GO-NH_2, dGO, and dGO-NH_2 suspensions do not present an irritant effect on RhE. By the same token, GO and GO-NH_2 powders were not irritant (Supplementary material, Figure S3). These findings are concordant with those obtained by other authors who evaluate the skin irritation potential of graphene-based materials using RhE models. For instance, Fusco *et al.* assessed the skin irritation potential of several graphene-based materials prepared with non-irritant exfoliation agents, observing that a single acute exposure of RhE to these nanomaterials in powder form does not induce skin irritation (Fusco et al., 2020). Also, Carlin *et al.* tested a variety of graphene related materials, including different GOs, concluding that these nanoparticles can be considered as non-irritant (Carlin et al., 2023). Experiments performed in mice were also in line with the observations made through *in vitro* tests (Sosa et al., 2023), confirming the suitability of RhE models to evaluate the irritation potential of nanomaterials. However, studies employing skin cell lines reported different conclusions, showing the ability of these materials to induce significant cytotoxicity in keratinocytes and skin fibroblasts (Liao et al., 2011; Pelin et al., 2017). These discrepancies could be explained due to the fact that the skin cell lines are simplified models that manage to reproduce essential skin functions, while RhE models simulate real skin tissue, presenting the different layers that exert barrier function against the nanomaterials, thus being more resistant to the toxic effect observed in skin cell assays.

5. Conclusions

Generating new toxicological data of graphene-derived materials along their life cycle is a relevant matter in the nanotechnology field, especially for those where the existing information is scarce, as it is case of GO-NH_2, or for less studied cellular models/exposure routes, such as the reconstructed skin model RhE. In this work, the safety of two graphene-based nanomaterials (GO and GO-NH_2) was evaluated in a comparative manner together with their respective degraded forms, aiming to elucidate whether structural modifications that pristine materials may suffer along their lifespan alter their potential hazard. With that objective, several *in vitro* assays using representative models for different exposure routes (A549 and HT29 cell lines, and a 3D model of a reconstructed human epidermis) were applied. The results obtained indicate that both GO-NH_2 and its degraded counterpart decreased the viability of the lung and colon cell lines, while GO and dGO were able to induce higher levels of ROS without affecting the cell viability. Moreover, the modifications that the materials suffered during their degradation process did not alter substantially their toxicological properties. dGO showed to have similar effects than GO, while dGO-NH_2 only caused a slightly higher decrease in the viability of A549 and HT29 cells than its pristine counterpart, but inducing lower levels of ROS. In the case of the tests carried out with the reconstructed skin model RhE, neither the studied pristine nanomaterials, nor their degraded forms, show irritant potential. The presented results provide novel insights into the toxicological potential that different graphene derivatives may have during their life cycle, through different exposure routes.

CRediT authorship contribution statement

Rocío Barros: Writing – original draft, Formal analysis. **Dalia de la Fuente-Vivas:** Writing – review & editing, Formal analysis. **Santiago Aparicio:** Writing – review & editing, Formal analysis. **Sonia Martel-Martín:** Writing – review & editing, Formal analysis. **Matteo Poddighe:** Writing – original draft, Investigation, Formal analysis. **Sebastiano Garroni:** Writing – review & editing, Investigation, Formal analysis. **Natalia Fernández-Pampín:** Writing – review & editing, Investigation, Formal analysis. **Juan Tamayo-Ramos:** Writing – review & editing, Supervision, Methodology, Investigation, Formal analysis, Conceptualization. **Carlos Rumbo:** Writing – review & editing, Writing – original draft, Supervision, Methodology, Investigation, Formal analysis, Conceptualization. **Sandra de la Parra:** Writing – review & editing, Writing – original draft, Investigation, Formal analysis.

Declaration of Competing Interest

The authors declare that they have no known competing financial interests or personal relationships that could have appeared to influence the work reported in this paper.

Data Availability

Data will be made available on request.

Acknowledgments

This work was supported by the Junta de Castilla y Leon-FEDER grant Nº BU058P20 (NANOCOMP), and by the European Union's H2020 research and innovation programme, under the grant agreement No 953152 (DIAGONAL). The scholarship of Matteo Poddighe received financial support within the activities of the PhD program in Chemical and Technological Sciences. We thank Graphenea for kindly providing us with the pristine GO and GO-NH_2 nanomaterials.

Appendix A. Supporting information

Supplementary data associated with this article can be found in the online version at doi:10.1016/j.tox.2024.153783.

References

Achawi, S., Pourchez, J., Feneon, B., Forest, V., 2021. Graphene-based materials in vitro toxicity and their structure-activity relationships: a systematic literature review. Chem. Res. Toxicol. 34, 2003–2018. https://doi.org/10.1021/acs.chemrestox.1c00243.

Ahmad, R.T.M., Hong, S.H., Shen, T.Z., Song, J.K., 2016. Water-assisted stable dispersal of graphene oxide in non-dispersible solvents and skin formation on the GO dispersion. Carbon 98, 188–194. https://doi.org/10.1016/j.carbon.2015.11.007.

Amrollahi-Sharifabadi, M., Koohi, M.K., Zayerzadeh, E., Hablolvarid, M.H., Hassan, J., Seifalian, A.M., 2018. In vivo toxicological evaluation of graphene oxide nanoplatelets for clinical application. Int. J. Nanomed. 13, 4757–4769. https://doi.org/10.2147/IJN.S168731.

Bacova, J., Knotek, P., Kopecka, K., Hromadko, L., Capek, J., Nyvltova, P., Bruckova, L., Schröterova, L., Sestakova, B., Palarcik, J., Motola, M., Cizkova, D., Bezrouk, A., Handl, J., Fiala, Z., Rudolf, E., Bilkova, Z., Macak, J.M., Rousar, T., 2022. Evaluating the use of TiO2 nanoparticles for toxicity testing in pulmonary A549 cells. Int. J. Nanomed. 17, 4211–4225. https://doi.org/10.2147/IJN.S374955.

Bengtson, S., Knudsen, K.B., Kyjovska, Z.O., Berthing, T., Skaug, V., Levin, M., Koponen, I.K., Shivayogimath, A., Booth, T.J., Alonso, B., Pesquera, A., Zurutuza, A., Thomsen, B.L., Troelsen, J.T., Jacobsen, N.R., Vogel, U., 2017. Differences in inflammation and acute phase response but similar genotoxicity in mice following

pulmonary exposure to graphene oxide and reduced graphene oxide. PLoS One 12, e0178355. https://doi.org/10.1371/journal.pone.0178355.
Bortolozzo, L.S., Côa, F., Khan, L.U., Medeiros, A.M.Z., Da Silva, G.H., Delite, F.S., Strauss, M., Martinez, D.S.T., 2021. Mitigation of graphene oxide toxicity in C. elegans after chemical degradation with sodium hypochlorite. Chemosphere 278, 130421. https://doi.org/10.1016/j.chemosphere.2021.130421.
Carlin, M., Garrido, M., Sosa, S., Tubaro, A., Prato, M., Pelin, M., 2023. In vitro assessment of skin irritation and corrosion properties of graphene-related materials on a 3D epidermis. Nanoscale 15, 14423–14438. https://doi.org/10.1039/d3nr03081d.
Cebadero-Domínguez, O., Ferrández-Gómez, B., Sánchez-Ballester, S., Moreno, J., Jos, A., Cameán, A.M., 2022. In vitro toxicity evaluation of graphene oxide and reduced graphene oxide on Caco-2 cells. Toxicol. Rep. 9, 1130–1138. https://doi.org/10.1016/j.toxrep.2022.05.010.
Chang, Y., Yang, S.T., Liu, J.H., Dong, E., Wang, Y., Cao, A., Liu, Y., Wang, H., 2011. In vitro toxicity evaluation of graphene oxide on A549 cells. Toxicol. Lett. 200, 201–210. https://doi.org/10.1016/j.toxlet.2010.11.016.
Chiticaru, E.A., Ionita, M., 2022. Graphene toxicity and future perspectives in healthcare and biomedicine. FlatChem 35, 100417. https://doi.org/10.1016/j.flatc.2022.100417.
Dąbrowski, B., Żuchowska, A., Brzózka, Z., 2023. Graphene oxide internalization into mammalian cells – a review. Colloids Surf. B Biointerfaces 221, 112998. https://doi.org/10.1016/j.colsurfb.2022.112998.
de la Parra, S., González, V., Solórzano Vives, P., Curiel-Alegre, S., Velasco-Arroyo, B., Rad, C., Barros, R., Tamayo-Ramos, J.A., Rumbo, C., 2022. Comparative toxicological assessment of three soils polluted with different levels of hydrocarbons and heavy metals using in vitro and in vivo approaches. Environ. Pollut. 315, 120472 https://doi.org/10.1016/j.envpol.2022.120472.
del Rio, B., Redruello, B., Linares, D.M., Ladero, V., Fernandez, M., Martin, M.C., Ruas-Madiedo, P., Alvarez, M.A., 2017. The dietary biogenic amines tyramine and histamine show synergistic toxicity towards intestinal cells in culture. Food Chem. 218, 249–255. https://doi.org/10.1016/j.foodchem.2016.09.046.
DiLeo, R.A., Landi, B.J., Raffaelle, R.P., 2007. Purity assessment of multiwalled carbon nanotubes by Raman spectroscopy. J. Appl. Phys., 064307 https://doi.org/10.1063/1.2712152.
Domenech, J., Hernández, A., Demir, E., Marcos, R., Cortés, C., 2020. Interactions of graphene oxide and graphene nanoplatelets with the in vitro Caco-2/HT29 model of intestinal barrier. Sci. Rep. 10, 2793. https://doi.org/10.1038/s41598-020-59755-0.
Domi, B., Bhorkar, K., Rumbo, C., Sygellou, L., Yannopoulos, S.N., Quesada, R., Tamayo-Ramos, J.A., 2020a. Fate assessment of commercial 2D MoS2aqueous dispersions at physicochemical and toxicological level. Nanotechnology 31, 445101. https://doi.org/10.1088/1361-6528/aba6b3.
Domi, B., Rumbo, C., García-Tojal, J., Sima, L.E., Negroiu, G., Tamayo-Ramos, J.A., 2020b. Interaction analysis of commercial graphene oxide nanoparticles with unicellular systems and biomolecules. Int. J. Mol. Sci. 21, 205. https://doi.org/10.3390/ijms21010205.
Drasler, B., Sayre, P., Steinhäuser, K.G., Petri-Fink, A., Rothen-Rutishauser, B., 2017. In vitro approaches to assess the hazard of nanomaterials. NanoImpact 8, 99–116. https://doi.org/10.1016/j.impact.2017.08.002.
Eivazzadeh-Keihan, R., Alimirzaloo, F., Aghamirza Moghim Aliabadi, H., Bahojb Noruzi, E., Akbarzadeh, A.R., Maleki, A., Madanchi, H., Mahdavi, M., 2022. Functionalized graphene oxide nanosheets with folic acid and silk fibroin as a novel nanobiocomposite for biomedical applications. Sci. Rep. 12, 6205. https://doi.org/10.1038/s41598-022-10212-0.
Fadeel, B., Bussy, C., Merino, S., Vázquez, E., Flahaut, E., Mouchet, F., Evariste, L., Gauthier, L., Koivisto, A.J., Vogel, U., Martín, C., Delogu, L.G., Buerki-Thurnherr, T., Wick, P., Beloin-Saint-Pierre, D., Hischier, R., Pelin, M., Candotto Carniel, F., Tretiach, M., Cesca, F., Benfenati, F., Scaini, D., Ballerini, L., Kostarelos, K., Prato, M., Bianco, A., 2018. Safety Assessment of Graphene-Based Materials: Focus on Human Health and the Environment. ACS Nano 12, 10582–10620. https://doi.org/10.1021/acsnano.8b04758.
Feng, W., Wang, J., Li, B., Liu, Y., Xu, D., Cheng, K., Zhuang, J., 2022. Graphene oxide leads to mitochondrial-dependent apoptosis by activating ROS-p53-mPTP pathway in intestinal cells. Int. J. Biochem. Cell Biol. 146, 106206 https://doi.org/10.1016/j.biocel.2022.106206.
Fernández-Pampín, N., González Plaza, J.J., García-Gómez, A., Peña, E., Garroni, S., Poddighe, M., Rumbo, C., Barros, R., Martel-Martín, S., Aparicio, S., Tamayo-Ramos, J.A., 2023. Toxicological assessment of pristine and degraded forms of graphene functionalized with MnOx nanoparticles using human in vitro models representing different exposure routes. Sci. Rep. 13, 11846 https://doi.org/10.1038/s41598-023-38993-y.
Ferrari, A.C., Meyer, J.C., Scardaci, V., Casiraghi, C., Lazzeri, M., Mauri, F., Piscanec, S., Jiang, D., Novoselov, K.S., Roth, S., Geim, A.K., 2006. Raman spectrum of graphene and graphene layers. Phys. Rev. Lett. 97, 187401 https://doi.org/10.1103/PhysRevLett.97.187401.
Filomeni, G., De Zio, D., Cecconi, F., 2015. Oxidative stress and autophagy: The clash between damage and metabolic needs. Cell Death Differ. 22, 377–388. https://doi.org/10.1038/cdd.2014.150.
Francisco, L.F.V., Baldivia, D. da S., Crispim, B. do A., Baranoski, A., Klafke, S.M.F.F., dos Santos, E.L., Oliveira, R.J., Barufatti, A., 2023. In vitro evaluation of the cytotoxic and genotoxic effects of Al and Mn in ambient concentrations detected in groundwater intended for human consumption. Ecotoxicol. Environ. Saf. 264, 115415 https://doi.org/10.1016/j.ecoenv.2023.115415.
Francisco, L.F.V., Baldivia, D., da, S., Crispim, B.D.A., Klafke, S.M.F.F., de Castilho, P.F., Viana, L.F., Dos Santos, E.L., de Oliveira, K.M.P., Barufatti, A., 2021. Acute toxic and genotoxic effects of aluminum and manganese using in vitro models. Toxics 9, 153. https://doi.org/10.3390/toxics9070153.
Fusco, L., Garrido, M., Martín, C., Sosa, S., Ponti, C., Centeno, A., Alonso, B., Zurutuza, A., Vázquez, E., Tubaro, A., Prato, M., Pelin, M., 2020. Skin irritation potential of graphene-based materials using a non-animal test. Nanoscale 12, 610–622. https://doi.org/10.1039/c9nr06815e.
Georgieva, M., Vasileva, B., Speranza, G., Wang, D., Stoyanov, K., Draganova-Filipova, M., Zagorchev, P., Sarafian, V., Miloshev, G., Krasteva, N., 2020. Amination of graphene oxide leads to increased cytotoxicity in hepatocellular carcinoma cells. Int. J. Mol. Sci. 21, 2427. https://doi.org/10.3390/ijms21072427.
Gies, V., Zou, S., 2018. Systematic toxicity investigation of graphene oxide: evaluation of assay selection, cell type, exposure period and flake size. Toxicol. Res. 7, 93–101. https://doi.org/10.1039/c7tx00278e.
Gurunathan, S., Kang, M.H., Jeyaraj, M., Kim, J.H., 2019. Differential cytotoxicity of different sizes of graphene oxide nanoparticles in leydig (TM3) and sertoli (TM4) cells. Nanomaterials 9, 139. https://doi.org/10.3390/nano9020139.
Han, S.G., Kim, J.K., Shin, J.H., Hwang, J.H., Lee, J.S., Kim, T.G., Lee, J.H., Lee, G.H., Kim, K.S., Lee, H.S., Song, N.W., Ahn, K., Yu, I.J., 2015. Pulmonary responses of sprague-dawley rats in single inhalation exposure to graphene oxide nanomaterials. Biomed. Res. Int. 2015, 376756 https://doi.org/10.1155/2015/376756.
He, F., Fan, J., Ma, D., Zhang, L., Leung, C., Chan, H.L., 2010. The attachment of Fe3O4 nanoparticles to graphene oxide by covalent bonding. Carbon N. Y. 11, 3139–3144. https://doi.org/10.1016/j.carbon.2010.04.052.
Jena, A.B., Samal, R.R., Bhol, N.K., Duttaroy, A.K., 2023. Cellular Red-Ox system in health and disease: The latest update. Biomed. Pharmacother. 162, 114606 https://doi.org/10.1016/j.biopha.2023.114606.
Jing, Q., Liu, W., Pan, Y., Silberschmidt, V.V., Li, L., Dong, Z.L., 2015. Chemical functionalization of graphene oxide for improving mechanical and thermal properties of polyurethane composites. Mater. Des. 85, 808–814. https://doi.org/10.1016/j.matdes.2015.07.101.
Jorio, A., Pimenta, M.A., Souza Filho, A.G., Saito, R., Dresselhaus, G., Dresselhaus, M.S., 2003. Characterizing carbon nanotube samples with resonance Raman scattering. N. J. Phys. 5, 139. https://doi.org/10.1088/1367-2630/5/1/139.
Keremidarska-Markova, M., Hristova-Panusheva, K., Andreeva, T., Speranza, G., Wang, D., Krasteva, N., 2018. Cytotoxicity Evaluation of Ammonia-Modified Graphene Oxide Particles in Lung Cancer Cells and Embryonic Stem Cells. Adv. Condens. Matter Phys. 2018, 9571828 https://doi.org/10.1155/2018/9571828.
Kim, Y.H., Jo, M.S., Kim, J.K., Shin, J.H., Baek, J.E., Park, H.S., An, H.J., Lee, J.S., Kim, B. W., Kim, H.P., Ahn, K.H., Jeon, K.S., Oh, S.M., Lee, J.H., Workman, T., Faustman, E. M., Yu, I.J., 2018. Short-term inhalation study of graphene oxide nanoplates. Nanotoxicology 12, 224–238. https://doi.org/10.1080/17435390.2018.1431318.
Krasteva, N., Keremidarska-Markova, M., Hristova-Panusheva, K., Andreeva, T., Speranza, G., Wang, D., Draganova-Filipova, M., Miloshev, G., Georgieva, M., 2019. Aminated graphene oxide as a potential new therapy for colorectal cancer. Oxid. Med. Cell. Longev. 2019, 3738980 https://doi.org/10.1155/2019/3738980.
Kucki, M., Rupper, P., Sarrieu, C., Melucci, M., Treossi, E., Schwarz, A., León, V., Kraegeloh, A., Flahaut, E., Vázquez, E., Palermo, V., Wick, P., 2016. Interaction of graphene-related materials with human intestinal cells: an in vitro approach. Nanoscale 8, 8749–8760. https://doi.org/10.1039/c6nr00319b.
Lalwani, G., D'Agati, M., Khan, A.M., Sitharaman, B., 2016. Toxicology of graphene-based nanomaterials. Adv. Drug Deliv. Rev. 105 (Pt B), 109–144. https://doi.org/10.1016/j.addr.2016.04.028.
Liao, C., Li, Y., Tjong, S.C., 2018. Graphene nanomaterials: synthesis, biocompatibility, and cytotoxicity. Int. J. Mol. Sci. 19, 3564. https://doi.org/10.3390/ijms19113564.
Liao, K.H., Lin, Y.S., MacOsko, C.W., Haynes, C.L., 2011. Cytotoxicity of graphene oxide and graphene in human erythrocytes and skin fibroblasts. ACS Appl. Mater. Interfaces 3, 2607–2615. https://doi.org/10.1021/am200428v.
Linares, D.M., Del Rio, B., Redruello, B., Ladero, V., Martin, M.C., Fernandez, M., Ruas-Madiedo, P., Alvarez, M.A., 2016. Comparative analysis of the in vitro cytotoxicity of the dietary biogenic amines tyramine and histamine. Food Chem. 197, 658–663. https://doi.org/10.1016/j.foodchem.2015.11.013.
Lowry, G.V., Gregory, K.B., Apte, S.C., Lead, J.R., 2012. Transformations of nanomaterials in the environment. Environ. Sci. Technol. 46, 6893–6899. https://doi.org/10.1021/es300839e.
Mukherjee, S.P., Gliga, A.R., Lazzaretto, B., Brandner, B., Fielden, M., Vogt, C., Newman, L., Rodrigues, A.F., Shao, W., Fournier, P.M., Toprak, M.S., Star, A., Kostarelos, K., Bhattacharya, K., Fadeel, B., 2018. Graphene oxide is degraded by neutrophils and the degradation products are non-genotoxic. Nanoscale 10, 1180–1188. https://doi.org/10.1039/c7nr03552g.
Ou, L., Song, B., Liang, H., Liu, J., Feng, X., Deng, B., Sun, T., Shao, L., 2016. Toxicity of graphene-family nanoparticles: A general review of the origins and mechanisms. Part. Fibre Toxicol. 13, 57. https://doi.org/10.1186/s12989-016-0168-y.
Papageorgiou, D.G., Kinloch, I.A., Young, R.J., 2017. Mechanical properties of graphene and graphene-based nanocomposites. Prog. Mater. Sci. 90, 75–127. https://doi.org/10.1016/j.pmatsci.2017.07.004.
Paredes, J.I., Villar-Rodil, S., Martínez-Alonso, A., Tascón, J.M.D., 2008. Graphene oxide dispersions in organic solvents. Langmuir 24, 10560–10564. https://doi.org/10.1021/la801744a.
Park, M.V.D.Z., Bleeker, E.A.J., Brand, W., Cassee, F.R., Van Elk, M., Gosens, I., De Jong, W.H., Meesters, J.A.J., Peijnenburg, W.J.G.M., Quik, J.T.K., Vandebriel, R.J., Sips, A.J.A.M., 2017. Considerations for Safe Innovation: The Case of Graphene. ACS Nano 11, 9574–9593. https://doi.org/10.1021/acsnano.7b04120.
Patel, K.D., Singh, R.K., Kim, H.W., 2019. Carbon-based nanomaterials as an emerging platform for theranostics. Mater. Horiz. 6, 434–469. https://doi.org/10.1039/c8mh00966j.

Pelin, M., Fusco, L., León, V., Martín, C., Criado, A., Sosa, S., Vázquez, E., Tubaro, A., Prato, M., 2017. Differential cytotoxic effects of graphene and graphene oxide on skin keratinocytes. Sci. Rep., 40572 https://doi.org/10.1038/srep40572.

Pelin, M., Sosa, S., Prato, M., Tubaro, A., 2018. Occupational exposure to graphene based nanomaterials: Risk assessment. Nanoscale 10, 15894–15903. https://doi.org/10.1039/c8nr04950e.

Rabchinskii, M.K., Ryzhkov, S.A., Kirilenko, D.A., Ulin, N.V., Baidakova, M.V., Shnitov, V.V., Pavlov, S.I., Chumakov, R.G., Stolyarova, D.Y., Besedina, N.A., Shvidchenko, A.V., Potorochin, D.V., Roth, F., Smirnov, D.A., Gudkov, M.V., Brzhezinskaya, M., Lebedev, O.I., Melnikov, V.P., Brunkov, P.N., 2020. From graphene oxide towards aminated graphene: facile synthesis, its structure and electronic properties. Sci. Rep. 10, 6902. https://doi.org/10.1038/s41598-020-63935-3.

Razaq, A., Bibi, F., Zheng, X., Papadakis, R., Jafri, S.H.M., Li, H., 2022. Review on graphene-, graphene oxide-, reduced graphene oxide-based flexible composites: from fabrication to applications. Materials 15, 1012. https://doi.org/10.3390/ma15031012.

Ren, S., Rong, P., Yu, Q., 2018. Preparations, properties and applications of graphene in functional devices: a concise review. Ceram. Int. 44, 11940–11955. https://doi.org/10.1016/j.ceramint.2018.04.089.

Rhazouani, A., Gamrani, H., El Achaby, M., Aziz, K., Gebrati, L., Uddin, M.S., Aziz, F., 2021. Synthesis and toxicity of graphene oxide nanoparticles: a literature review of in vitro and in vivo studies. Biomed. Res. Int. 2021, 5518999 https://doi.org/10.1155/2021/5518999.

Ruiz, O.N., Fernando, K.A.S., Wang, B., Brown, N.A., Luo, P.G., McNamara, N.D., Vangsness, M., Sun, Y.P., Bunker, C.E., 2011. Graphene oxide: a nonspecific enhancer of cellular growth. ACS Nano 5, 8100–8107. https://doi.org/10.1021/nn202699t.

Saiful Badri, M.A., Salleh, M.M., Md Noor, N.F. ain, Rahman, M.Y.A., Umar, A.A., 2017. Green synthesis of few-layered graphene from aqueous processed graphite exfoliation for graphene thin film preparation. Mater. Chem. Phys. 193, 212–219. https://doi.org/10.1016/j.matchemphys.2017.02.029.

Sattar, T., 2019. Current Review on Synthesis, Composites and Multifunctional Properties of Graphene. Top. Curr. Chem. 377, 10. https://doi.org/10.1007/s41061-019-0235-6.

Schneider, T., Westermann, M., Glei, M., 2017. In vitro uptake and toxicity studies of metal nanoparticles and metal oxide nanoparticles in human HT29 cells. Arch. Toxicol. 91, 3517–3527. https://doi.org/10.1007/s00204-017-1976-z.

Seabra, A.B., Paula, A.J., De Lima, R., Alves, O.L., Durán, N., 2014. Nanotoxicity of graphene and graphene oxide. Chem. Res. Toxicol. 27, 159–168. https://doi.org/10.1021/tx400385x.

Selvaraj, S.K., Ramesh, R., Narendhra, T.M.V., Agarwal, I.N., Chadha, U., Paramasivam, V., Palanisamy, P., 2021. New developments in carbon-based nanomaterials for automotive brake pad applications and future challenges. J. Nanomater. 2021, 6787435 https://doi.org/10.1155/2021/6787435.

Sengupta, J., 2020. Application of carbon nanomaterials in the electronic industry. : Handb. Nanomater. Manuf. Appl. 421–450. https://doi.org/10.1016/B978-0-12-821381-0.00017-X.

Sergent, J.A., Paget, V., Chevillard, S., 2012. Toxicity and genotoxicity of Nano-SiO2 on human epithelial intestinal HT-29 cell line. Ann. Occup. Hyg. 56, 622–630. https://doi.org/10.1093/annhyg/mes005.

Shamsi, S., Alagan, A.A., Sarchio, S.N.E., Md Yasin, F., 2020. Synthesis, characterization, and toxicity assessment of Pluronic F127-functionalized graphene oxide on the embryonic development of Zebrafish (Danio rerio). Int. J. Nanomed. 15, 8311–8329. https://doi.org/10.2147/IJN.S271159.

Shvedova, A.A., Pietroiusti, A., Fadeel, B., Kagan, V.E., 2012. Mechanisms of carbon nanotube-induced toxicity: Focus on oxidative stress. Toxicol. Appl. Pharmacol. 261, 121–133. https://doi.org/10.1016/j.taap.2012.03.023.

Sohaebuddin, S.K., Thevenot, P.T., Baker, D., Eaton, J.W., Tang, L., 2010. Nanomaterial cytotoxicity is composition, size, and cell type dependent. Part. Fibre Toxicol. 7, 22. https://doi.org/10.1186/1743-8977-7-22.

Sosa, S., Tubaro, A., Carlin, M., Ponti, C., Vázquez, E., Prato, M., Pelin, M., 2023. Assessment of skin sensitization properties of few-layer graphene and graphene oxide through the Local Lymph Node Assay (OECD TG 442B). NanoImpact 29, 100448. https://doi.org/10.1016/j.impact.2022.100448.

Sukhanova, A., Bozrova, S., Sokolov, P., Berestovoy, M., Karaulov, A., Nabiev, I., 2018. Dependence of nanoparticle toxicity on their physical and chemical properties. Nanoscale Res. Lett. 13, 44. https://doi.org/10.1186/s11671-018-2457-x.

Vimalanathan, B., Vijaya, J.J., Mary, B.C.J., Ignacimuthu, S., Daniel, M., Jayavel, R., Bououdina, M., Bellucci, S., 2022. The anticancer efficacy of thiourea-mediated reduced graphene oxide nanosheets against human colon cancer cells (HT-29). J. Funct. Biomater. 13, 130. https://doi.org/10.3390/jfb13030130.

Wroblewska, A., Duzynska, A., Judek, J., Stobinski, L., Zeranska, K., Gertych, A.P., Zdrojek, M., 2017. Statistical analysis of the reduction process of graphene oxide probed by Raman spectroscopy mapping. J. Phys. Condens. Matter 29, 475201. https://doi.org/10.1088/1361-648X/aa92fe.

Yang, K., Gong, H., Shi, X., Wan, J., Zhang, Y., Liu, Z., 2013. In vivo biodistribution and toxicology of functionalized nano-graphene oxide in mice after oral and intraperitoneal administration. Biomaterials 34, 2787–2795. https://doi.org/10.1016/j.biomaterials.2013.01.001.

Yu, W., Sisi, L., Haiyan, Y., Jie, L., 2020. Progress in the functional modification of graphene/graphene oxide: A review. RSC Adv. 10, 15328–15345. https://doi.org/10.1039/d0ra01068e.

Zare-Zardini, H., Taheri-Kafrani, A., Ordooei, M., Amiri, A., Karimi-Zarchi, M., 2018. Evaluation of toxicity of functionalized graphene oxide with ginsenoside Rh2, lysine and arginine on blood cancer cells (K562), red blood cells, blood coagulation and cardiovascular tissue: In vitro and in vivo studies. J. Taiwan Inst. Chem. Eng. 93, 70–78. https://doi.org/10.1016/j.jtice.2018.08.010.

Zaytseva, O., Neumann, G., 2016. Carbon nanomaterials: Production, impact on plant development, agricultural and environmental applications. Chem. Biol. Technol. Agric. 3, 17. https://doi.org/10.1186/s40538-016-0070-8.

Zhang, L., Xia, J., Zhao, Q., Liu, L., Zhang, Z., 2010. Functional graphene oxide as a nanocarrier for controlled loading and targeted delivery of mixed anticancer drugs. Small 6, 537–544. https://doi.org/10.1002/smll.200901680.